ISSN 1063-7826, Semiconductors, 2015, Vol. 49, No. 4, pp. 461–471. © Pleiades Publishing, Ltd., 2015.
Original Russian Text © A.V. Sachenko, A.E. Belyaev, N.S. Boltovets, P.N. Brunkov, V.N. Jmerik, S.V. Ivanov, L.M. Kapitanchuk, R.V. Konakova, V.P. Klad'ko, P.N. Romanets, P.O. Saja, N.V. Safryuk, V.N. Sheremet, 2015, published in Fizika i Tekhnika Poluprovodnikov, 2015, Vol. 49, No. 4, pp. 472–482.

SEMICONDUCTOR STRUCTURES, LOW-DIMENSIONAL SYSTEMS, AND QUANTUM PHENOMENA

Temperature Dependences of the Contact Resistivity in Ohmic Contacts to n^+-InN

A. V. Sachenko[a], A. E. Belyaev[a], N. S. Boltovets[b], P. N. Brunkov[c, d], V. N. Jmerik[c], S. V. Ivanov[c], L. M. Kapitanchuk[e], R. V. Konakova[a]^, V. P. Klad'ko[a], P. N. Romanets[a], P. O. Saja[a], N. V. Safryuk[a], and V. N. Sheremet[a]

[a] *Lashkaryov Institute of Semiconductor Physics, National Academy of Sciences, pr. Nauki 41, Kyiv, 03028 Ukraine*
^e-mail: konakova@isp.kiev.ua
[b] *"Orion" Research Institute, vul. E. Pottier 8a, Kyiv, 03057 Ukraine*
[c] *Ioffe Physical–Technical Institute, Russian Academy of Sciences, ul. Politekhnicheskaya 26, St. Petersburg, 194021 Russia*
[d] *National Research University of Information Technologies, Mechanics and Optics, pr. Kronverkskii 49, St. Petersburg, 197101 Russia*
[e] *Paton Electric Welding Institute, National Academy of Sciences of Ukraine, vul. Bozhenko 11, Kyiv, 03680 Ukraine*

Submitted July 31, 2014; accepted for publication September 4, 2014

Abstract—The temperature dependences of the contact resistivity (ρ_c) of ohmic contacts based on the Au–Ti–Pd–InN system are measured at an InN doping level of 2×10^{18} cm^{-3} in the temperature range of 4.2–300 K. At temperatures $T > 150$ K, linearly increasing dependences $\rho_c(T)$ are obtained. The dependences are explained within the mechanism of thermionic current flow through metal shunts associated with dislocations. Good agreement between theoretical and experimental dependences is achieved assuming that the flowing current is limited by the total resistance of the metal shunts, and the density of conductive dislocations is $\sim 5 \times 10^9$ cm^{-2}. Using the X-ray diffraction method, the density of screw and edge dislocations in the structure under study is measured: their total density exceeds 10^{10} cm^{-2}.

DOI: 10.1134/S1063782615040193

1. INTRODUCTION

In the last few years, indium nitride and alloys on its basis have been the most actively studied materials among nitrides of Group-III elements. Interest in them is due to promising applications in the development of some active elements for opto-, spin-, and microwave electronics [1–4]. The specific feature of these materials is their epitaxial growth technology. The point is that there is no substrate material for them, as well as for other III–N compounds, which would be suitable for commercial production; therefore, InN and alloys on its basis are grown as heterostructures with buffer layers. As substrates, Al_2O_3, GaAs, Si, and fianites are used. Due to the mismatch of the lattice parameters and thermal expansion coefficients of the InN film and substrate (e.g., Al_2O_3), internal mechanical stresses arise in heterostructures, whose relaxation leads to the generation of dislocations with densities from 10^8 to 3×10^{11} cm^{-2}. This cannot but affect the parameters of corresponding devices, first and foremost, the characteristics of ohmic contacts to them.

Indeed, as shown in [5–7], the contact resistivity ρ_c of ohmic contacts to semiconductors with high dislocation densities and its temperature dependence $\rho_c(T)$ depend heavily on the dislocation density, if the contact-forming metal (alloy) or metal from other contact metallization layers penetrates into the thin near-contact semiconductor layer via dislocations during ohmic-contact formation, forming metal shunts in it. Furthermore, as shown in [8], in layers of InN, due to its thermodynamic instability and the specificity of epitaxial growth near the transition to surface enrichment with the metal, the formation of metal In precipitates and In accumulation at dislocations is highly probable. This can also cause the formation of metal shunts in InN layers.

The dependence $\rho_c(T)$ at rather high temperatures can be an increasing dependence. In this case, ρ_c increases with measurement temperature and, in the region of operating temperatures, can appreciably exceed ρ_c measured at room temperature. Goldberg et al. (see, e.g., [5]) proposed an explanation of the increasing dependences $\rho_c(T)$ by the temperature dependence of the metal-shunt resistance. However, the proposed explanation does not describe the dependence $\rho_c(T)$ in a rather wide range of temperature measurements. For example, in the region of rather low temperatures, the dependences $\rho_c(T)$ are either decreasing or independent of temperature. The behavior of the experimental dependences $\rho_c(T)$ in semi-

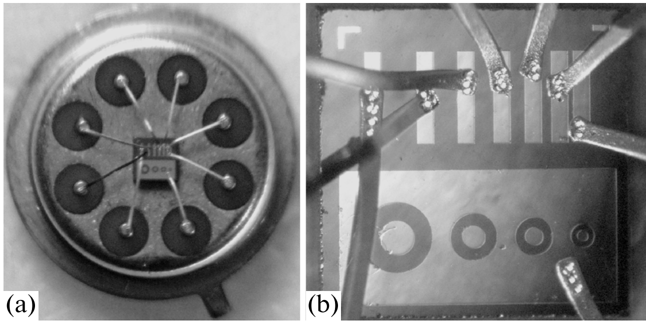

Fig. 1. (a) Test structure for measuring the dependence $\rho_c(T)$ in the housing and (b) the test structure fragment.

conductors with high dislocation densities in a rather wide temperature range was fully explained in [6, 7]. In addition to the shunt resistance, the resistance which appears during electron transfer from the semiconductor to the shunt ends was considered. It was shown that accumulation band bending takes place in the near-contact region of the semiconductor due to high electric-field strengths at the boundaries of the ends with the semiconductor. In this case, the diffusion theory of current flow in semiconductors can be valid in some cases: the flowing current is directly proportional and the resistivity is inversely proportional to the electron mobility, which explains the temperature dependences $\rho_c(T)$ in a rather wide temperature range.

Without a doubt, the formation of the ohmic contact and the current flow mechanism in it depend on the doping level of the semiconductor near-contact region [9]. The data presented in the table show that low-resistance ohmic contacts to n-InN and alloys on its basis are as a rule observed in the presence of degenerate layers of the semiconductor in the near-contact region (for n-InN, the concentration should exceed the effective density of states in the conduction band, $>5.1 \times 10^{17}$ cm^{-3} [10]). The table is compiled using the data of [11–24].

The systematic research of the temperature dependence $\rho_c(T)$ of ohmic contacts to n-InN has barely been carried out. We found only four papers of two teams of authors [13, 14, 18, 23], in which the properties of ohmic contacts to n-InN were studied in the temperature ranges of 223–398 K [13, 14, 18] and 4.2–400 K [23]. In [14, 18], measurements were performed only above room temperature. In [23], measurements were carried out in the temperature range $T =$ 4.2–400 K. According to [23], an increasing dependence of the contact resistivity R_c in the ohmic contact to an InN nanowire was observed, which the authors attempted to explain by the metallic conductivity in degenerate InN. No direct measurements of $\rho_c(T)$ were performed in [23]. We note that n-InN layers with a donor concentration of $\gtrsim 10^{20}$ cm^{-3} were used in [13, 14, 18]; the room-temperature ρ_c was (1.0–1.87) $\times 10^{-7}$ Ω cm^2 in the best samples. In this case, the role of the high density of dislocations generated in similar heterostructures in the charge-transport mechanism was not considered in the cited papers (see table).

In the present work, the temperature dependence ρ_c of ohmic contacts to n-InN layers grown on Al_2O_3 substrates with a GaN buffer layer, with a dislocation density above 10^8 cm^{-2}, is experimentally studied in the temperature range of 4.2–300 K. The results obtained are explained within the approach developed in [6, 7].

2. SAMPLES AND EXPERIMENTAL

Ohmic contacts were formed by the sequential vacuum deposition of metals onto an InN(0.6 μm)–GaN(0.9 μm)–Al_2O_3(400 μm) heterostructure heated to 350°C. An Au(500 nm)–Ti(60 nm)–Pd(30 nm)–n-InN ohmic contact was formed during metal deposition and was not additionally annealed. The parameters of InN–GaN–Al_2O_3 heterostructures grown by plasma-activated molecular-beam epitaxy were identical to those of similar structures studied in [25]. InN(0001) was grown on a GaN buffer layer preliminarily formed on an Al_2O_3 substrate. The free electron density in the n-InN was ~(1.5–3.0) $\times 10^{18}$ cm^{-3}, the mobility was (1300–2000) cm^2 V^{-1} s^{-1}. We studied the samples with continuous metallization to measure the profiles of the distribution of contact metallization components by Auger electron spectrometry using a LAS-2000 spectrometer. The contact resistivity was measured on planar test structures by the transmission line method (TLM) in the temperature range $T =$ 4.2–300 K. The contact length and width were $L = 75$ μm and $W = 400$ μm, the spaces between the contact pads were 150, 100, 80, 60, 40, and 20 μm. To measure the dependences $\rho_c(T)$, the test structures were mounted into a case (see Fig. 1). The temperature was stabilized by a UTREKS k25v system.

The dislocation density in the heterostructure and the phase composition of the Pd–Ti–Au contact metallization layers were measured by X-ray diffraction methods. To obtain information on the structural quality (dislocation density) and the strain state of the samples, a wide region of reciprocal space was scanned using an X'Pert PRO MRD XL (PANalytical B.V., Almelo, The Netherlands) high-resolution diffractometer. Both the symmetric (0002) and asymmetric $(11\bar{2}4)$, $(12\bar{3}3)$, and $(10\bar{1}5)$ reflections of GaN and AlN were analyzed. For the same reflections, two-dimensional reciprocal space maps (RSMs) were measured. It was found that the screw- and edge-dislocation densities in n-InN are ~2.3×10^8 and ~3.4×10^{10} cm^{-2}, respectively. X-ray diffraction (XRD) measurements of the contact metallization were performed with an ARL X'Tra (Thermo scientific) setup

Ohmic contacts to n-InN layers and alloys on its basis

Metallization	Semiconductor	Carrier concentration, cm^3 (at InN layer thickness d, μm)	Annealing	ρ_c, Ω cm^2	Note	References
1	2	3	4	5	6	7
Ti(250 Å)/Pt(500 Å)/Au(3000 Å)	InN/GaAs	5×10^{19}	350–525°C, forming gas	$(5–6) \times 10^{-7}$		[11]
Ti(200 Å)/Al(1000 Å)	InN/GaN	10^{19} (5×10^{-3})	Electron-beam evaporation (e-beam)	6×10^{-5}	InN/GaN superlattice	[12]
Ti(500 Å)/Pt(750 Å)/Au(3000 Å)	InN/GaAs	$>10^{20}$ (0.12)	RTA 300–410°C/60 s	1.86×10^{-7} at 300 K, 4.47×10^{-7} at 430 K	ρ_c was measured in the range of 297–430 K	[13]
Ti(500 Å)/Pt(750 Å)/Au(3000 Å)	InN/GaAs/InN/InGaAs/GaAs	5×10^{20} (0.12)	Electron-beam evaporation (e-beam)	1.8×10^{-7} 5×10^{-7}	Bipolar transistor	[14]
Ti(250 Å)/Pt(500 Å)/Au(1000 Å)	InGaN/GaN/GaAs	10^{19}	RTA: 400, 700, 800, 900°C/30 s in N_2	10^{-7}	Cubic phase of alloy	[15]
Au/Ge/Ni				10^{-7}		
WSi$_x$(1000 Å)				2×10^{-5} after RTA 700°C/30 s		
W(1000 Å)/WSi$_x$(1000 Å) Ti(200 Å)/Al(1000 Å)	InN/GaAs	10^{20} (0.2)	RTA 300–500°C	1.1×10^{-7} after RTA 400°C; 2×10^{-7}, without annealing	ρ_c increases with annealing temperature, ρ_c is minimum in the initial samples	[16]
W(1000 Å)	$In_{0.65}Ga_{0.35}N$/GaAs	10^{19} (0.2)	RTA 300–900°C	4.5×10^{-8}	Annealing at 600°C	
WSi$_x$(1000 Å)				1.8×10^{-7}		
Ti(200 Å)/Al(1000 Å)				3.5×10^{-7}		
W(1000 Å)	$In_{0.75}Al_{0.25}N$/GaAs	8×10^{18} (0.2)	RTA 500–900°C	1.2×10^{-2}	Without annealing	
WSi$_x$(1000 Å)				2×10^{-3}		
Ti(200 Å)/Al(1000 Å)				6×10^{-4}		
WSi$_x$	InN/InAlN/AlN/Al_2O_3	$(1–3) \times 10^{20}$ (0.5–0.5)		4.8×10^{-4} 3.6×10^{-5} 3.5×10^{-6}	Effect of technological growth conditions of InN on Al_2O_3 and on GaAs (temperature is 525–575°C, N flux is 5–20 sccm)	[17]
	InN/InAlN/AlN/GaAs			$(8–9) \times 10^{4}$		
	InAlN/AlN/Al_2O_3	$(1–3) \times 10^{19}$ (0.3–0.5)		1.9×10^{-5}	Technological growth conditions	
	InAlN/AlN/GaAs			1.4×10^{-5}		
W(1000 Å)	InN/GaAs	10^{20} (0.2)	300–500°C/30 s in N_2	10^{-7}, annealing 400°C	$\rho_c(T)$ measurements in the range of 223–398 K	
WSi$_x$(1000 Å)				2×10^{-7}, without annealing		
Ti(200 Å)/Al(1000 Å)				2.5×10^{-7}, without annealing		

(Contd.)

1	2	3	4	5	6	7
W(1000 Å)	InGaN/GaAs	10^{19} (0.2)	RTA: 600–900°C/15 s in N_2	4×10^{-8} after RTA 600°C	$\rho_c(T)$ measurements in the range of 223–398 K	[18]
WSi_x(1000 Å)				2×10^{-7}, without annealing		
Ti(200 Å)/Al(1000 Å)	InAlN/GaAs	8×10^{18} (0.2)	RTA: 500–900°C/15 s in N_2	3×10^{-7}, annealing at 600°C	$\rho_c(T)$ measurements in the range of 223–398 K	
W(1000 Å)				1.5×10^{-2}, without annealing		
WSi_x(1000 Å)				10–3, RTA: 500°C/15 s		
Ti(200 Å)/Al(1000 Å)				6×10^{-5}, without annealing		
W(1000 Å)	InN/GaAs	10^{20} (0.2)	RTA: 300–500°C/15 s in N_2	$<10^{-7}$ after RTA 600°C; 10^{-7} at 300 K after RTA	$\rho_c(T)$ measurements in the range of 223–398 K	[19]
$WSi_{0.44}$(1000 Å)	InN/GaAs			10^{-6}		
W(1000 Å)	InGaN/GaAs	10^{19} (0.2)	RTA: 600–900°C	4×10^{-8} after RTA 600°C		
WSi_x(1000 Å)				2×10^{-7}, without annealing		
WSi_x	InN/InAlN/AlN/Al_2O_3	(0.05)	Annealing: 300–700°C/5 min in N_2	3×10^{-6} after annealing at 300°C ($d = 0.2$ μm)	As the InN-film thickness increases, ρ_c decreases after annealing at 300°C	[20]
		(0.1)		10^{-5} after annealing at 300°C ($d = 0.05$ μm)		
		(0.2)		6×10^{-6} after annealing at 300°C ($d = 0.1$ μm)		
W(600 Å)	InGaN/GaN/Al_2O_3	1.63×10^{19}, doped with Si (0.13)	*e*-beam, RTA: 500–950°C/90 s in N_2	4×10^{-8} after RTA 950°C		[21]
Ti(1000 Å)/Au(2000 Å)	InN/AlN/Al_2O_3	2.14×10^{18}	*e*-beam, without annealing	1.42×10^{-7}	InN thickness from 10 nm to 1 μm	[22]
Al(1000 Å)/Au(2000 Å)		1.49×10^{18}		1.86×10^{-6}		
Ni(1000 Å)/Au(2000 Å)		2.28×10^{18}		1.04×10^{-6}		
Pd(5 nm)/Ti(20 nm)/Pt(20 nm)/Au(100 nm)	InN/Si	$>10^{20}$	*e*-beam	1.8×10^{-7}	ρ_c to InN film	[23]
				1.09×10^{-7}	ρ_c to nanowire, nanocontact R_c is measured in the range of 4.2–400 K	
Ti(200 Å)/Al(400 Å)/Ni(200 Å)/Au(800 Å)	InN/Al_2O_3	3×10^{18} (0.5)	RTA: 300–500°C/60 s in N_2	6×10^{-6}	After RTA at 400°C	[24]
Ti(200 Å)/Al(400 Å)/TiB_2(200 Å)/Au(800 Å)				1.6×10^{-6}		

RTA is rapid thermal annealing.

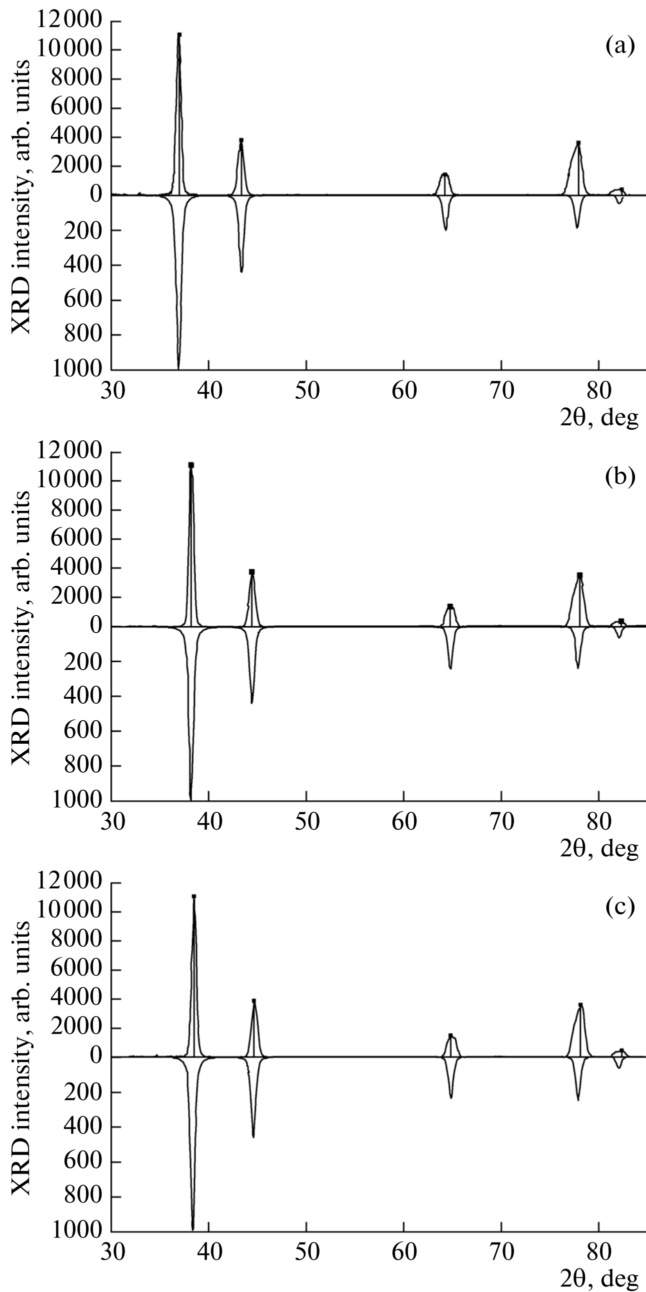

Fig. 2. Experimental X-ray diffraction pattern of the contact metallization and calculated X-ray diffraction patterns of (a) Ti, (b) $Au_{0.919}Ti_{0.081}$, and (c) Au (vertical lines indicate the positions of the experimental peaks).

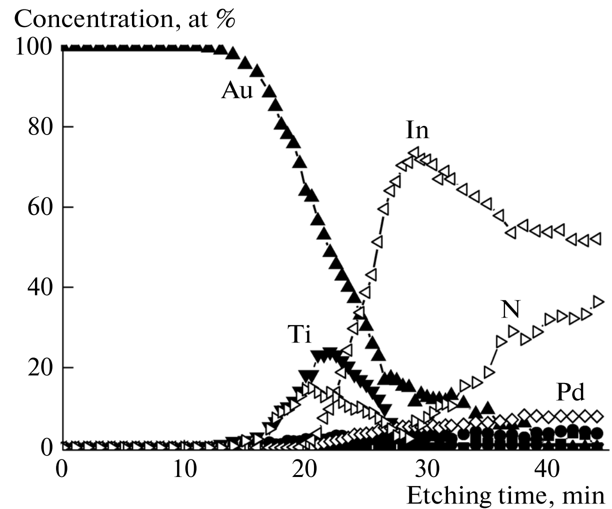

Fig. 3. Profiles of the distribution of Au–Ti–Pd–n^+-InN contact-metallization layer components.

using CuK_λ radiation. The tube voltage and current were 45 kV and 30 mA. The diffraction spectra were recorded using the sliding beam method. The measurements were performed in the step mode with a scanning step of 0.030° and a point acquisition time of 1 s. Phase analysis was performed using the ICDD PDF-2 database (2012 release).

According to the XRD data, Ti was detected in the contact metallization (Pdf Number 010-88-2321, see Fig. 2). The reflection-peak broadening at large angles indicates the presence of either Au (Pdf Number 010-77-9662) or the $Au_{0.919}Ti_{0.081}$ compound (Pdf Number 010-74-5407). We note that these materials are very close in lattice parameters.

At the same time, it is known that titanium forms intermetallic compounds with gold even at 350°C [26], hence, the probability of $Au_{0.919}Ti_{0.081}$ compound formation in the case of metal deposition onto a substrate heated to 350°C is rather high. As for palladium, no reflections corresponding to it or its compounds were detected. This is explainable under the assumption that palladium is in an amorphous state in the system under study. The presence of palladium is confirmed by Auger electron spectrometry (Fig. 3).

Using scanning electron microscopy (SEM), cleavages of the Au–Ti–Pd–InN–GaN–Al_2O_3 contact structures were studied. A columnar structure for both the GaN buffer layer and InN film with characteristic defects in the InN–GaN interface region is observed in the micrograph in Fig. 4. The linear density of vertical defects in InN and GaN is ~10^4 and ~7×10^4 cm^{-1}, respectively.

3. MEASUREMENT RESULTS AND DISCUSSION

The current–voltage (I–V) characteristics of the contacts under study were linear and symmetric in the entire measured temperature range.

The experimental temperature dependence ρ_c is shown in Fig. 5 (dots). Its behavior differs significantly from the typical dependences $\rho_c(T)$ for non-rectifying (ohmic) Schottky contacts in which, depending on the doping level in the near-contact semiconductor layer, ρ_c is either independent of temperature (tunneling

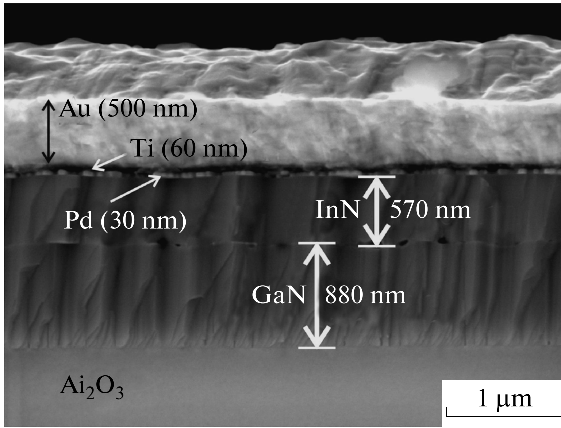

Fig. 4. SEM image of the cleavage surface of the Au–Ti–Pd–InN–GaN–Al_2O_3 contact structure.

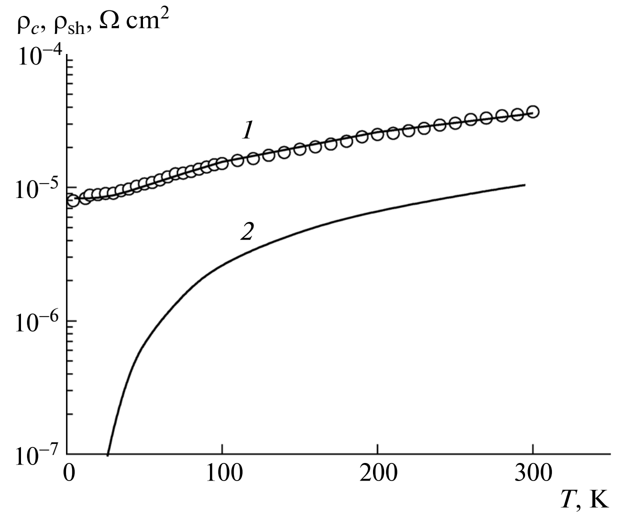

Fig. 5. Experimental (dots *1*) and calculated (solid curve *1*) dependences $\rho_c(T)$ of the Au–Ti–Pd–n^+-InN ohmic contact and (*2*) the dependence of the shunt resistivity $\rho_{sh}(T)$.

charge-transport mechanism) or decreases with temperature (thermal-field or thermionic charge-transport mechanism). In the case at hand, ρ_c increases with temperature in the entire range of temperature measurements: at low temperatures (from 0 to 30 K), ρ_c increases very slightly; in the temperature range of 30–150 K, $\rho_c \propto T^{0.6}$; at temperatures >150 K, $\rho_c \sim T$. Charge transport theories existing before [6, 7] did not explain this dependence $\rho_c(T)$ in metal–semiconductor contacts.

In theoretical modeling of the experimental dependence $\rho_c(T)$ of the ohmic contact to n^+-InN, shown in Fig. 5, we take into account that the semiconductor is degenerate in this case. Let us suppose that charge transport occurs over metal shunts associated with dislocations. To calculate $\rho_c(T)$, we use the expressions given in [6], valid for the case of degenerate semiconductors.

In the case of degeneracy, the following expression for the contact resistivity ρ_{te} is valid for the thermionic current-flow mechanism [6]

$$\rho_{te} = \frac{k}{qA(m/m_0)T\ln[1+\exp(z+y_{c0})]}, \qquad (1)$$

where k is the Boltzmann constant, q is the elementary charge, A is the Richardson constant, m is the electron effective mass, m_0 is the free electron mass, T is the temperature, and y_{c0} is the dimensionless (normalized to kT) contact potential. The dimensionless Fermi energy $z = E_F/kT$ in the case at hand is determined from the bulk neutrality equation

$$N_d = \frac{2}{\sqrt{\pi}}N_{c0}\left(\frac{T}{300}\right)^{3/2}\int_0^{\infty}\frac{x^{0.5}}{1+\exp(x-z)}dx, \qquad (2)$$

where N_d is the donor concentration, N_{c0} is the effective electron density of states in the InN conduction band at $T = 300$ K.

The contact resistivity ρ_{tw}, taking into account the fact that not all of the contact area is involved in current flow through the shunts, is given by

$$\rho_{tw} = \frac{\rho_{te}}{\pi L_D^2 N_D}, \qquad (3)$$

where L_D is the Debye screening length and N_D is the density of conductive dislocations.

In the case of strong degeneracy, the Debye screening length L_D in the semiconductor tends to r_0 which is independent of temperature and weakly depends on the doping level N_D,

$$r_0 = \frac{1}{2}\left(\frac{\pi}{3}\right)^{1/6}\left(\frac{4\pi\varepsilon_0\varepsilon_s\hbar^2}{mq^2N_d^{1/3}}\right)^{1/2}. \qquad (4)$$

In the case of arbitrary degeneracy, the Debye screening length L_D in the semiconductor is given by [27]

$$L_D = \left(\frac{\varepsilon_0\varepsilon_s kT}{2q^2N_{c0}}\right)^{0.5}[\Phi'_{1/2}(z)]^{-1/2}, \qquad (5)$$

where

$$\Phi'_{1/2}(z) = \frac{2}{\sqrt{\pi}}\int_0^{\infty}\frac{\sqrt{x}\exp(x-z)}{[1+\exp(x-z)]^2}dx, \quad z = E_F/kT.$$

Since the total resistance of all metal shunts is connected in series with ρ_{tw} in the case of a degenerate semiconductor, the total resistance of the ohmic con-

tact in the semiconductor with a high dislocation density can be written as

$$\rho_c = \rho_{tw} + \rho_{sh}, \quad (6)$$

where $\rho_{sh} = R_{sh}(T)/N_D$, $R_{sh}(T) = \rho_0(T)d_D/\pi r^2$ is the temperature dependence of the metal-shunt resistivity, ρ_0 is the resistivity, d_D is the dislocation length, and r is the shunt radius (in the calculation, all shunts are considered as identical). In this case, it is assumed that the current flowing between dislocations can be neglected in comparison with the current flowing through dislocations, which is provided by the high barrier between dislocations [6].

The temperature dependence $\rho_{sh}(T)$, taking into account the temperature dependence of the resistivity of the contact-forming metal (palladium), according to the handbook [28], in a wide temperature range (from 0 to 300 K) behaves as follows. At $T = 0$K, the resistance of the normal (not superconducting) metal is equal to the residual resistance R_s. Then the resistance increases by the law $\propto T^5$ (see Fig. 5, curve *2*), which is caused by electron scattering at phonons [29]. Then the transition region follows, the resistance $\propto T^n$, where n rapidly decreases. Finally, at $T \geq T_D$, where T_D is the Debye temperature, $n = 1$, i.e., the metal resistance linearly increases with temperature.

All above expressions correspond to the whole contact area.

Theoretical curve *1* for the dependence $\rho_c(T)$, shown in Fig. 5, was calculated by formula (6) using the InN parameters given in [1, 10, 30]. As seen in Fig. 5, the calculated dependence of the contact resistivity ρ_c coincides with the experimental data. This is achieved using the following parameters: $N_D \approx 5 \times 10^9$ cm^{-2}, $r = 5 \times 10^{-8}$ cm, and $d_D \sim 0.1$ μm. It should be noted that, since $R_{sh} \propto d_D/r^2$, there is a certain ambiguity in the determination of d_D and r. For example, r also increases with d_D.

We note that the revealed total density of screw and edge dislocations substantially exceeds that necessary for implementing the mechanism under consideration.

As seen in Fig. 5, the contact resistivity ρ_c at $T =$ 300 K is $\sim 3 \times 10^{-5}$ Ω cm^2 in the case at hand. According to the data in the table, the values of ρ_c obtained for degenerate InN vary from 10^{-4} to 10^{-6} Ω cm^2. In the studies [13, 23] performed using InN with a doping level of $>10^{20}$ cm^{-3}, it was reported that $\rho_c \sim 10^{-7}$ Ω cm^2. In these works, the temperature dependences of ρ_c were increasing. In [13, 23] the specific mechanism of the implementation of the contact resistivity was not discussed, although tunneling was indicated as a possible ρ_c formation mechanism in [13].

We note that estimation of the contact resistivity in highly degenerate InN contacts by the Padovani–Stratton formula [31]

$$\rho_c(T) = \frac{E_{00}}{q^2 n_0 V_T}\left[\exp\left(\frac{\varphi_b - E_{f0}}{E_{00}(T)}\right)\right], \quad (7)$$

where $E_{00} = 0.054[(m_0/m)(n_0/10^{20})(11.7/\varepsilon_s)]^{0.5}$, V_T is a value on the order 10^7 cm/s, for $n_0 = 5 \times 10^{20}$ cm^{-3}, $m = 0.24m_0$, and $\varphi_b = 0.7$ V, yields $\sim 10^{-10}$ Ω cm^2 which is smaller than the observed values by three orders of magnitude. We note that renormalization of the effective electron mass in InN from $0.07m_0$ to $0.24m_0$ [10] accounts for the InN conduction-band nonparabolicity at high degeneracy.

Close values are obtained in estimating ρ_c by formula (1). This suggests that the experimentally determined values of ρ_c in the case of highly degenerate InN cannot be explained assuming that the entire contact area is involved in current transport through the contact. However, this result is well explained in the case where the current is transferred through an area smaller by approximately three orders of magnitude. This condition is reached if the current flows through the shunts associated with dislocations, and the dislocation density $N_D \gtrsim 10^{11}$ cm^{-2}. As direct estimations based on the contact-resistivity formation mechanism proposed in [6] show, the typical values of ρ_c shown in the table are implemented exactly in this case. According to [32], such values of N_D in InN are quite achievable. However, in this case, the question as to why the current does not flow between dislocations should be answered. A possible answer is that there is an electron repulsing potential in the InN near-contact region, whose nature differs from the Schottky band bending. This can be the total potential of high-density charged dislocations in the interface plane [33]. In this case, potentials of isolated dislocations overlap and produce a large averaged repulsive band bending. At the same time, shunts associated with dislocations "pierce" this negatively charged region with the result that current flow through them remains possible.

In [23], based on highly degenerate InN with a doping level of $>10^{20}$ cm^{-3}, nanowires ~100 nm in diameter were fabricated, and the temperature dependences of the total resistivity of the contacts and nanowire were measured. An attempt was made to explain the increasing (linear) dependences by the metallic behavior of highly degenerate InN. It should be noted that the physics of conductivity formation in metals and highly degenerate semiconductors, associated with carrier scattering in the region of rather high temperatures by optical phonons varies. For example, as shown above, the metal resistivity at very low temperatures increases by the law $\propto T^5$; above the Debye temperature, it increases by linear law. In degenerate III–V semiconductors at low temperatures, the elec-

tron mobility μ_n is independent of temperature and is mainly controlled by scattering at impurities [34]; at rather high temperatures, it decreases, generally speaking, nonlinearly due to scattering at optical phonons. In this case, the resistivity of highly degenerate semiconductors will increase also nonlinearly.

Let us calculate the mobility of a highly degenerate electron gas in a degenerate semiconductor. For a degenerate semiconductor in the temperature range where the Fermi energy is much higher than the thermal energy ($E_F \gg kT$), the equilibrium distribution function over the energy E can be approximated by the Heaviside step function $\Theta(E_F - E)$. If the doping level is rather high, the Mott transition in the impurity band already has occurred, and donor ionization will be complete independent of temperature. In other words, the impurity- and conduction bands overlap. The latter means that the electron density n is defined by the Fermi momentum p_F: $n = N_D = p_F^3/(3\pi^2\hbar^3)$. It is convenient to describe the conduction-band nonparabolicity using the model [35]

$$E(p) = \frac{p_s^2}{m}\left(\sqrt{1 + \left(\frac{p}{p_s}\right)^2} - 1\right), \tag{8}$$

where the characteristic momentum $p_s^2 = mE_s/2$. In this case, $E_s \approx E_g$, where E_g is the band gap. To avoid confusion, we note that the relation of the Fermi momentum with the Fermi energy is $E(p_F) = E_F$. Using the kinetic equation in the weak field approximation for calculating the conductivity σ and defining the mobility as $\mu_n = \sigma/(qn)$, we obtain the expression for the mobility of the degenerate electron gas in the form

$$\mu_n = \frac{q\tau_m(E_F)}{m\sqrt{1 + (p_F/p_s)^2}}, \tag{9}$$

where $\tau_m(E_F)$ is the momentum relaxation time calculated for the Fermi energy.

The partial contributions of various electron-momentum-relaxation mechanisms, $\tau_m^{-1}(E_F) = \sum_j \tau_{jm}^{-1}(E_F)$, are summed in the same way as the partial contributions of the mobilities, $\mu^{-1}(E_F) = \sum_j \mu_j^{-1}(E_F)$. The most significant momentum-relaxation mechanisms at high doping levels are carrier scattering at a charged impurity and the interaction of electrons with optical phonons. The methods for calculating the corresponding relaxation times $\tau_i(E)$ and $\tau_{opt}(E)$ can be found, e.g., in [36, 37]. In what follows, we present the expression for corresponding mobilities. The carrier mobility for scattering at a charged impurity is given by

$$\mu_i = \left\{\frac{m^2q^3}{3\pi\hbar^3}\left(\frac{1}{4\pi\varepsilon_s\varepsilon_0}\right)^2\left[1 + \left(\frac{p_F}{p_s}\right)^2\right] \times \left(\ln\left|1 + \frac{4p_F^2}{\hbar^2\lambda_{TF}^{-2}}\right| - \frac{4p_F^2}{4p_F^2 + \hbar^2\lambda_{TF}^{-2}}\right)\right\}^{-1}, \tag{10}$$

where $\lambda_{FT} = [2q^2mp_F\sqrt{1 + (p_F/p_s)^2}/(\varepsilon_s\varepsilon_0\pi^2\hbar^3)]^{-1/2}$ is the Thomas–Fermi screening length.

We note that expression (10) is independent of temperature. A perturbation such as an optical phonon results in a local change in the electric polarization vector. The mobility accounting for scattering at optical phonons is given by the formula [37]

$$\mu_{opt} = \left\{\frac{qm^2\hbar\omega_0(\varepsilon_d^{-1} - \varepsilon_s^{-1})}{4\pi\varepsilon_0\hbar^2}\sqrt{1 + \left(\frac{p_F}{p_s}\right)^2} N\left(\frac{\hbar\omega_j}{kT}\right) \times \left[\xi_{jF}^{+}\ln\left|\frac{p_F + p_s\sqrt{\xi_{jF}^{+2} - 1}}{p_F - p_s\sqrt{\xi_{jF}^{+2} - 1}}\right| + \exp\left(\frac{\hbar\omega_j}{kT}\right) \times \xi_{jF}^{-}\ln\left|\frac{p_F + p_s\sqrt{\xi_{jF}^{-2} - 1}}{p_F - p_s\sqrt{\xi_{jF}^{-2} - 1}}\right|\Theta(\xi_{jF}^{-} - 1)\right]\right\}^{-1}, \tag{11}$$

where $\xi_{jF}^{\pm} = \sqrt{1 + (p_F/p_s)^2} \pm m\hbar\omega_j/p_s^2$, $\hbar\omega_{opt}$ is the optical phonon energy, ε_d and ε_s are the steady-state and dynamic permittivities, and $N(x)$ is the Planck distribution function.

Figures 6a and 6b show the calculated temperature dependences of the electron mobility μ_n for degenerate InN, constructed by the formula

$$\mu_n = (\mu_i^{-1} + \mu_{opt}^{-1} + \mu_{pl}^{-1})^{-1}, \tag{12}$$

for the absolute $\mu_n(T)$ and relative $\mu_n(T)/\mu_n(300)$ mobilities. In the calculation, we used the following material parameters: the effective mass $m = 0.07m_0$, the steady-state permittivity $\varepsilon_s = 15.3$, the dynamic permittivity $\varepsilon_d = 7.5$, the optical phonon energy $\hbar\omega_{opt} = 73$ meV, and the band nonparabolicity parameter $E_s = 0.5$ eV. We can see that the higher the doping level, the closer the law of the mobility decrease to the linear one at rather high temperatures.

The parameter of the calculated curves is the doping level. As seen in the figure, at the doping level $n_0 \approx 2 \times 10^{18}$ cm^{-3}, the slope of the temperature dependences of the mobility in the region $T > 100$ K, normalized to μ_n ($T = 300$ K), is worse described by linear law than at a doping level of 5×10^{18} cm^{-3}. At the same time, at a doping level of 5×10^{20} cm^{-3}, the linear approximation rather well describes the mobility slope

at $T > 150$ K. It is natural that the mobility slope close to the linear law corresponds to a linear increase in the resistivity of the highly degenerate semiconductor, $R(T) = R_0[1 + \alpha_{\text{eff}}(T - T_0)]$. Thus, for highly degenerate semiconductors, the metal-like, rather than metallic nature of the dependence $R(T)$ should be considered. The temperature resistance coefficient α_{eff}, in contrast to the temperature coefficient α in metals, where the typical value is $\alpha \approx 1/273$ K^{-1}, decreases with decreasing μ_n ($T = 0$) and increasing m. As a result, at higher degeneracy levels, α_{eff} in semiconductors is approximately ten times lower than in metals.

We note that in the case considered in [23], where only the total resistivity R was measured,

$$R = 2R_c + \frac{\rho_s L_s}{\pi r_s^2}, \tag{13}$$

where R_c is the contact resistivity, $\rho_s = (nq\mu_n)^{-1}$ is the degenerate nanocontact resistivity, r_s and L_s are its radius and length, we can obtain additional information on R_c and $R_s = \rho_s L_s/\pi r_s^2$, if we take into account that the relations

$$R_c = R_{m0}[1 + \alpha(T - T_0)], \tag{14}$$

$$R_s = R_{s0}[1 + \alpha_{\text{eff}}(T - T_0)] \tag{15}$$

are valid, where $R_{c0} = \rho_{tw}/\pi r_s^2$, R_{m0} is the total resistance of all metal shunts and threading dislocations at $T = T_0$, and R_{s0} is the nanowire resistance at $T = T_0$.

Supposing that $T_0 = 300$ K, we can write for $T >$ 150 K that

$$\begin{aligned} 2(R_{c0} + R_{m0}) + R_{s0} &= 2150\ \Omega, \\ \alpha_{\text{eff}} + \alpha(2R_{m0}/R_{s0}) &= 4.7 \times 10^{-4}\ \text{K}^{-1}. \end{aligned} \tag{16}$$

As a result, we have two equations and three unknowns: R_{c0}, R_{m0}, and R_{s0}. In turn, $R_{s0} = \rho_{s0}L_s/\pi r_s^2$, where ρ_{s0} is the nanowire resistivity; as a result, only two unknowns remain in Eqs. (16). As preliminary estimations show, $R_{m0} \ll R_{c0}$ and $R_{m0} \ll R_{s0}$; therefore, R_{m0} can be disregarded to a first approximation. Substituting the nanowire parameters and two extreme (lower and upper) values of ρ_{s0}, equal to 2.5×10^{-4} and 5.5×10^{-4} Ω cm, respectively, according to [23], into the expression for R_{s0}, we obtain $R_{s0}^{1} = 1548$ Ω and $R_{s0}^{11} = 3406$ Ω. The second value should be rejected, since it does not satisfy the first equation of (16). Then, substituting R_{s0}^{1} into this equation, we obtain $2R_{c0} \approx 600$ Ω. At the same time, R_{c0} can be determined by the formula $R_{c0} = \rho_{tw}/\pi r_s^2$. Substituting the shunt density of 5×10^{11} cm^{-2} and the doping level of 5×10^{20} cm^{-3} in calculating ρ_{tw} by formula (3), we obtain $2R_{c0} \approx 600$ Ω which corresponds to the above value.

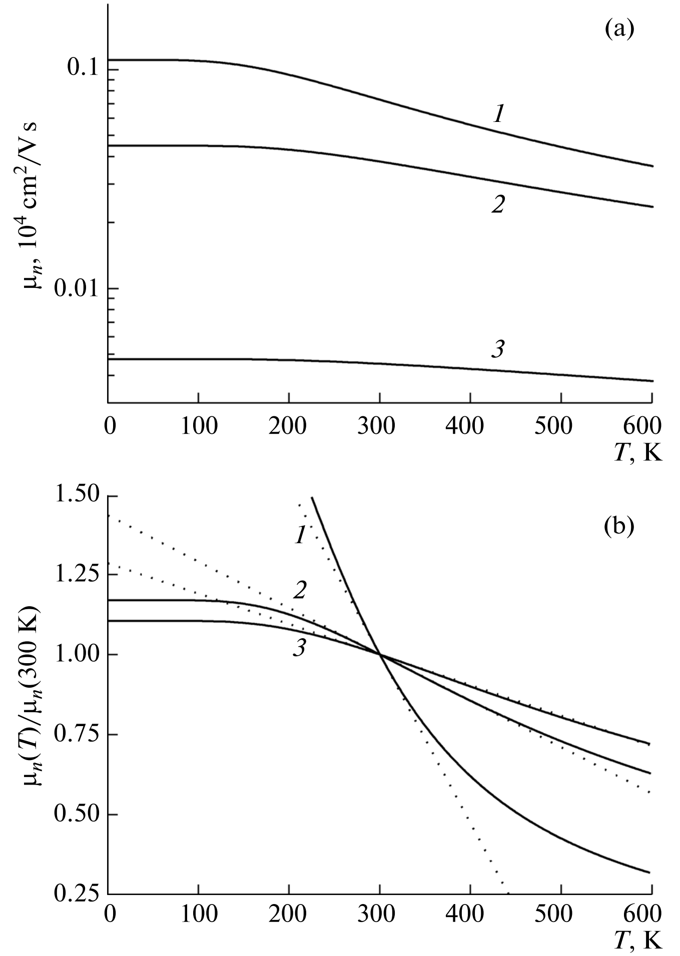

Fig. 6. Temperature dependences $\mu_n(T)$ of the electron mobility in degenerate InN at various doping levels n_0: (*1*) 2×10^{18}, (*2*) 5×10^{18}, and (*3*) 5×10^{20} cm^{-3}. (a) Mobilities in absolute units, (b) the same dependences normalized to the mobility at $T = 300$ K and their linear approximation (dashed curves).

The above formulas for the degenerate-gas mobility with the parameters of highly degenerate InN yield values very close to the experimental ones for doping levels up to 10^{21} cm^{-3} [38] (see Fig. 7a). We note that quantitative description of the experimental dependences of the mobility requires consideration of the Hartree–Fock term and corrections to the electron spectrum (see, e.g., [39]), and more correct calculation of screening effects (see [36]). Since all these factors lead to an increase in the effective electron mass, for simplicity, we modeled these effects of overestimated conduction-band nonparabolicity. In view of this fact, we obtained $\mu_n \sim 51$ cm^2/V s ($T = 300$ K) at a doping level of 5×10^{20} cm^{-3}. This value is rather close to the maximum possible value of 50 cm^2/Vs, obtained when using $\rho_s = 2.5 \times 10^{-4}$ Ω cm given in [23]

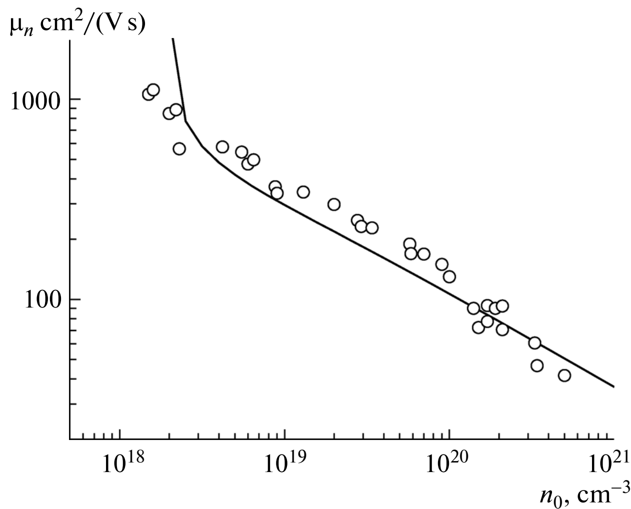

Fig. 7. Temperature dependence $\mu_n(T)$ of the electron mobility in degenerate InN on the doping level at room temperature: the experimental data (dots) are taken from [38], the curve is our calculation.

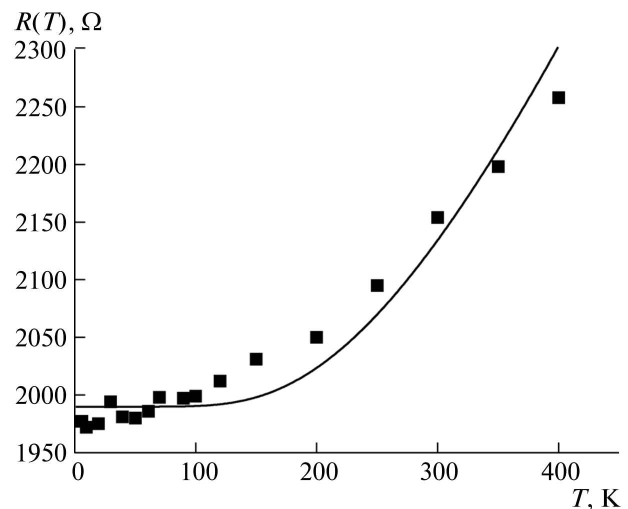

Fig. 8. Temperature dependence of the resistance $R(T)$: experimental data [23] (dots) and calculation for a nanocontact from [23]: (solid curve).

(taking into account the ρ_s error). In this case, the slope of the temperature dependence $\mu_n(T)$ is very close to 4.7×10^{-4} K^{-1} given in [23]; the value of R_{s0} at the used parameters is 1548 Ω.

Figure 8 shows the experimental dependence $R(T)$ taken from [23] (dots) and the theoretical dependence obtained using formulas (8)–(13) (solid curve) taking into account the above considerations. The nanocontact base is an n-InN nanowire ($N_D = 5 \times 10^{20}$ cm^{-3}) 7 μm long and 120 nm in diameter. The doubled contact resistance was set equal to 600 Ω. We can see rather good agreement between the experimental and calculated data.

In this case, the contribution of the contact resistance R_c of both contacts to the total resistance R is ~28%; the value of the latter is mostly due to the nanowire resistance. Recalculation of the contact resistance R_c to the contact resistivity yields 3×10^{-8} Ω cm^2. This value of ρ_c is a record low and is significantly lower than all contact resistivities listed in the table. The contact resistivity of 1.09×10^{-7} Ω cm^2 given in [23] in fact corresponds to the total resistance of the nanowire and two contacts, multiplied by the contact area.

In conclusion, we note that the accuracy of the contact-resistivity estimates in the case described in [23] is much worse than the accuracy of the contact resistivity calculated for a material with a doping level of 2×10^{18} cm^{-3}. The relative error of ρ_c determination in the case of highly degenerate InN is no less than 35%. This is due to the rather low accuracy of material-resistivity determination and incomplete information about some other parameters. In particular, according to [23], the nanowire length varied from 7 to 10 μm; at the same time, it is not indicated what the length was for the structure measurement results given in Fig. 4 of this study. At the same time, the main conclusion we made when analyzing the results given in [23] remains valid, i.e., in reality the contact resistivity obtained in [23] is ~3×10^{-8} Ω cm^2 which is much lower than the value presented in that paper.

4. CONCLUSIONS

It was shown that the increasing dependences of the contact resistivity $\rho_c(T)$ we obtained for ohmic contacts to InN can be explained by current flow through dislocations associated with metal shunts. The linear increase in ρ_c is caused by the temperature dependence of the shunt resistance.

It was confirmed that the linear temperature dependence of the total resistance of the nanowire and contact resistances of highly degenerate InN, obtained in [23], is caused by the close-to-linear temperature dependence of the nanowire resistance. However, we explained this dependence within the mechanism of electron scattering at optical phonons, which leads, in particular, to other values of the coefficient of the temperature dependence of the resistivity, than in metals.

It was shown that the contact resistivity ρ_c correctly estimated based on the data of [23], taking into account the smallness of R_c in comparison with R_{s0}, is a record low for InN-based contacts and is much lower than that given in [13], being 3×10^{-8} Ω cm^2.

REFERENCES

1. V. Yu. Davydov and A. A. Klochikhin, Semiconductors **38**, 861 (2004).

2. *Indium Nitride and Related Alloys*, Ed. by T. D. Veal, C. F. McConville, and W. J. Achaff (CRS Press, Boca Raton, 2010).
3. A. N. Kovalev, *Transistors Based on Semiconductor Heterostructures* (Izd. Dom MISiS, Moscow, 2011) [in Russian].
4. S. V. Ivanov, D. V. Nechaev, A. A. Sitnikova, V. V. Ratnikov, M. A. Yagovkina, N. V. Rzheutskii, E. V. Lutsenko, V. N. Jmerik, Semic. Sci. Technol. **29** (8), 084008 (2014).
5. T. V. Blank and Yu. A. Goldberg, Semiconductors **41**, 1263 (2007).
6. A. V. Sachenko, A. E. Belyaev, N. S. Boltovets, R. V. Konakova, Ya. Ya. Kudryk, S. V. Novitskii, V. N. Sheremet, J. Li, and S. A. Vitusevich, J. Appl. Phys. **111**, 083701 (2012).
7. A. V. Sachenko, A. E. Belyaev, N. S. Boltovets, A. O. Vinogradov, V. P. Kladko, R. V. Konakova, Ya. Ya. Kudryk, A. V. Kuchuk, V. N. Sheremet, and S. A. Vitusevich, J. Appl. Phys. **112**, 063703 (2012).
8. S. V. Ivanov, T. V. Shubina, T. A. Komissarova, and V. N. Jmerik, J. Cryst. Growth **403**, 83 (2014).
9. S. M. Sze and K. K. Ng, *Physics of Semiconductor Devices*, 3rd ed. (Wiley, New Jersey, 2007).
10. P. Rinke, M. Scheffler, A. Qteish, M. Wnkelnkemper, D. Bimberg, and J. Neugebauer, Appl. Phys. Lett. **89**, 161919 (2006).
11. C. R. Abernathy, S. J. Pearton, F. Ren, and P. W. Wisk, J. Vac. Sci. Technol. B **11**, 179 (1993).
12. M. E. Lin, F. J. Huang, and H. Morkoc, Appl. Phys. Lett. **64**, 2557 (1994).
13. F. Ren, C. R. Abernathy, S. J. Pearton, and P. W. Wisk, Appl. Phys. Lett. **64**, 1508 (1994).
14. F. Ren, C. R. Abernathy, S. N. G. Chu, J. R. Lothian, and S. J. Pearton, Appl. Phys. Lett. **66**, 1503 (1995).
15. A. Durba, S. J. Pearton, C. R. Abernathy, J. W. Lee, P. H. Holloway, and F. Ren, J. Vac. Sci. Technol. B **14**, 2582 (1996).
16. C. B. Varthli, S. J. Pearton, C. R. Abernathy, J. D. MacKenzie, R. J. Shul, J. C. Zolper, M. L. Lovejoy, A. G. Baca, and M. Hagerott-Crawford, J. Vac. Sci. Technol. B **14**, 3520 (1996).
17. S. M. Donovan, J. D. MacKenzie, C. R. Abernathy, S. J. Pearton, F. Ren, K. Jones, and M. Cole, Appl. Phys. Lett. **70**, 2592 (1997).
18. F. Ren, C. B. Vartuli, S. A. Pearton, C. R. Abernathy, S. M. Donovan, J. D. MacKenzie, R. J. Shul, J. C. Zolper, M. L. Lovejoy, A. G. Boy, M. Hagerott-Crawford, and K. A. Jones, J. Vac. Sci. Technol. A **15**, 802 (1997).
19. C. B. Vartuli, S. J. Pearton, C. R. Abernathy, J. D. MacKenzie, M. L. Lovejoy, R. J. Shul, Z. C. Zolper, A. G. Baca, M. Hagerot-Crawford, A. Jones, and F. Ren, Solid-State Electron. **41**, 531 (1997).
20. S. M. Donovan, J. D. MacKenzie, C. R. Abernathy, S. J. Pearton, F. Ren, K. Jones, and M. Cole, Solid-State Electron. **42**, 1831 (1998).
21. Han-Ki Kim, Ja-Soon Jang, Seong-Ju Park, and Tac-Jeon Seong, J. Electrochem. Soc. **147**, 1573 (2000).
22. H. Lu, W. J. Schaff, L. F. Eastman, and C. E. Stutz, Appl. Phys. Lett. **82**, 1736 (2003).
23. Chin-Yang Chang, Gou-Chung Chi, Wei-Ming Wang, Li-Chyong Chen, Kuei-Hsien Chen, F. Ren, and S. J. Pearton, Appl. Phys. Lett. **87**, 093112 (2005).
24. Rohit Khanna, B. P. Gila, L. Stafford, S. J. Pearton, F. Ren, I. I. Kravchenko, Amir Dabiran, and A. Osinsky, Appl. Phys. Lett. **90**, 162107 (2007).
25. M. E. Rudinsky, A. A. Gutkin, and P. N. Brunkov, Semiconductors **44**, 1020 (2010).
26. N. Cheng, H. von Seefeld, and M.-A. Nicolet, in *Proceedings of the Symposium on Thin Films Interfaces and Interactions*, Ed. by J. E. E. Baglin and J. M. Poate (Princeton Univ. Press, Princeton, NJ, 1980), Vol. 80, p. 323.
27. V. Bonch-Bruevich and S. Kalashnikov, *Semiconductor Physics* (Nauka, Moscow, 1990) [in Russian].
28. P. M. Malkov, I. B. Danilin, A. G. Zel'dovich, and A. B. Fradkov, *Handbook of Physical and Technical Fundamentals of Cryogenics* (Energiya, Moscow, 1973) [in Russian].
29. J. Bardeen, J. Appl. Phys. **11**, 88 (1940).
30. *Properties of Advanced Semiconductor Materials GaN, AlN, InN, BN, SiC, SiGe,* Ed. by M. M. Levinshtein, S. L. Rumyantsev, and M. S. Shur (Wiley, New York, 2001).
31. F. A. Padovani and R. Stratton, Solid State Electron. **9**, 695 (1966).
32. V. V. Mamutin, N. A. Cherkashin, V. A. Vekshin, V. N. Zhmerik, and S. V. Ivanov, Phys. Solid State **43**, 151 (2001).
33. H. F. Matare, *Defect Electronics in Semiconductors* (Wiley-Interscience, New York, 1971).
34. V. I. Fistul', *Heavily Doped Semiconductors* (Plenum Press, New York, 1969).
35. I. M. Dykman, V. M. Rosenbaum, and F. T. Vasko, Phys. Status Solidi B **88**, 385 (1978).
36. V. F. Gantmakher and I. B. Levinson, *Carrier Scattering in Metals and Semiconductors* (Nauka, Moscow, 1984; North-Holland, Amsterdam, 1987).
37. K. Seeger, *Semiconductor Physics* (Springer, Wien, 1973).
38. C. Rauch, F. Tuomisto, P. D. C. King, T. D. Veal, H. Lu, and W. J. Schaff, Appl. Phys. Lett. **101**, 011903 (2012).
39. K.-F. Berggren and B. E. Sernelius, Phys. Rev. B **24**, 1971 (1981).

Translated by A. Kazantsev